Structural Characterization and Formation Mechanism of Sitting-Atop (SAT) Complexes of 5,10,15,20-Tetraphenylporphyrin with Divalent Metal Ions. Structure of the Cu(II)−SAT Complex As Determined by Fluorescent Extended X-ray Absorption Fine Structure

Yasuhiro Inada,[†] Yuko Nakano,[‡] Masahiko Inamo,[§] Masaharu Nomura,[||] and Shigenobu Funahashi*[,‡]

Laboratory of Analytical Chemistry, Graduate School of Science, Chikusa, Nagoya University, Nagoya 464-8602, Japan, Research Center for Materials Science, Nagoya University, Chikusa, Nagoya 464-8602, Japan, Department of Chemistry, Aichi University of Education, Igaya, Kariya 448-8542, Aichi, Japan, and Photon Factory, Institute of Materials Structure Science, High Energy Accelerator Research Organization, Oho, Tsukuba 305-0801, Japan

Received May 2, 2000

The UV−vis absorption spectra and the formation kinetics of sitting-atop (SAT) complexes ($M(H_2tpp)^{2+}$) of 5,10,15,20-tetraphenylporphyrin (H_2tpp) with a series of divalent metal ions (M^{2+} = Mn^{2+}, Fe^{2+}, Co^{2+}, Ni^{2+}, Cu^{2+}, and Zn^{2+}) in acetonitrile have been investigated. The structural characteristics of the SAT complexes for a series of M^{2+} ions are discussed on the basis of the UV−vis absorption spectra. The structure parameters around Cu^{2+} in the Cu(II)−SAT complex were determined by a fluorescent EXAFS method: the coordination number is 6 with three kinds of Cu−N interactions having bond lengths of 2.05, 1.98, and 2.32 Å for pyrrolenine nitrogens of H_2tpp, acetonitrile nitrogens at equatorial sites, and acetonitrile nitrogens at axial sites, respectively. The rate constants at 25 °C for the formation of the SAT complex in acetonitrile are as follows: k_f/mol^{-1} kg s^{-1} = 3.4×10^2 for Mn^{2+}, 0.18 for Co^{2+}, 1.6×10^{-3} for Ni^{2+}, and 61 for Zn^{2+}. The finding that the variation trends in the rate constants for a series of M^{2+} ions for the SAT complex formation and the solvent exchange reaction in various solvents are very similar indicates that the rate-determining step for the SAT complex formation is the interchange between the coordinating nitrogen of a bound acetonitrile and the pyrrolenine nitrogen of H_2tpp. The fact that the values of k_f are smaller by 4−6 orders of magnitude in comparison with those of the solvent exchange suggests that there is a large energetic loss due to the fast preequilibria prior to the rate-determining step, such as deformation of a porphyrin ring and outer-sphere encounter formation due to an electrostatic interaction between M^{2+} and the local negative charge on the pyrrolenine nitrogens. We observed the subsequent formation of the corresponding metalloporphyrins by deprotonation of the SAT complex and oxidation of the M^{2+} center, of which the dynamic behavior was significantly different for the different M^{2+} ions.

Introduction

Many metalloporphyrins and analogues play significant roles in vivo, and the metalloporphyrin formation reaction is one of the most important processes in biological systems in relation to the biosynthesis of heme.[1−7] However, the mechanism is not well established not only in biological systems but also for simple systems in vitro. In 1960, Fleisher and Wang proposed that an intermediate should exist during the processes of metalloporphyrin formation, and this intermediate was called a sitting-atop (SAT) complex, in which two pyrrolenine nitrogens coordinate to the metal ion and two protons on the pyrrole nitrogens still remain.[8] Hereafter, some SAT complexes as an intermediate were reported, prepared from hematoporphyrin IX and chloroplatinate(II) in aprotic solvents[9] and from tetraphenylporphyrin and copper(II) in the presence of triphenylphosphine in microemulsion media.[10] However, because the corresponding SAT intermediates have not been directly detected in the kinetic studies of the metalloporphyrin formation reaction, the reaction mechanism and the SAT intermediate are still not fully clarified.

Recently, we detected the SAT complex formed by the reaction between Cu^{2+} and 5,10,15,20-tetraphenylporphyrin (H_2tpp) in acetonitrile (AN, "an" as a ligand).[11,12] This first direct detection of the SAT complex ($Cu(H_2tpp)^{2+}$) was achieved by

* To whom correspondence should be addressed. E-mail: sfuna@chem4.chem.nagoya-u.ac.jp.
[†] Research Center for Materials Science, Nagoya University.
[‡] Laboratory of Analytical Chemistry, Nagoya University.
[§] Aichi University of Education.
[||] High Energy Accelerator Research Organization.

(1) Lavallee, D. K. *Mol. Struct. Energ.* **1988**, *9*, 279.
(2) Blackwood, M. E., Jr.; Rush, T. S., III.; Medlock, A.; Dailey, H. A.; Spiro, T. G. *J. Am. Chem. Soc.* **1997**, *119*, 12170.
(3) Lloyd, S. G.; Franco, R.; Moura, J. J. G.; Moura, I.; Ferreira, G. C.; Huynh, B. H. *J. Am. Chem. Soc.* **1996**, *11*, 9892.
(4) Conn, M. M.; Prudent, J. R.; Schultz, P. G. *J. Am. Chem. Soc.* **1996**, *118*, 7012.
(5) Taketani, S. *Regulation of Heme Protein Synthesis*; Fujita, H., Ed.; AlphaMed Press: Dayton, Ohio, 1994.
(6) Dailey, H. A. *Biosynthesis of Heme and Chlorophylls*; McGraw-Hill: New York, 1990.
(7) Lavallee, D. K. *The Chemistry and Biochemistry of N-Substituted Porphyrins*; VCH: New York, 1987.
(8) Fleischer, E. B.; Wang, J. H. *J. Am. Chem. Soc.* **1960**, *82*, 3498.
(9) Macquet, J. P.; Theophanides, T. *Can. J. Chem.* **1973**, *51*, 219.
(10) Letts, K.; Mackay, R. A. *Inorg. Chem.* **1975**, *14*, 2993.
(11) Inada, Y.; Sugimoto, Y.; Nakano, Y.; Itoh, Y.; Funahashi, S. *Inorg. Chem.* **1998**, *37*, 5519.
(12) Coordinated solvent molecules in complexes are not involved in the formula for simplicity except for specific expression.

10.1021/ic000479w CCC: $19.00
Published on Web 09/22/2000

the strategic use of AN as a solvent with very weak basicity. In the overall process of the metalloporphyrin formation reaction between M^{n+} and H_2tpp,

$$M^{n+} + H_2tpp \rightleftarrows M(tpp)^{(n-2)+} + 2H^+ \quad (1)$$

at least two steps should be involved, i.e., the coordination of the pyrrolenine nitrogens of H_2tpp to M^{n+} and the deprotonation of the pyrrole protons. To thoroughly elucidate the metalation mechanism, kinetic observations for each step are needed. Prevention of the deprotonation of the pyrrole protons is achieved by the appropriate selection of solvents with a low Brønsted basicity because released protons cannot be stabilized in such a solvent. In addition, the stabilization of the SAT complex formation is enhanced in solvents with a low Lewis basicity because such solvation of M^{n+} is weaker. In these connections, the selection of AN as a solvent has been the best to separate the two steps and to directly detect the SAT complex formed during the metalloporphyrin formation reaction. To unify the reaction mechanisms of the SAT complex formation and the overall metalation of the porphyrin, our studies on the SAT complexes have been extended to reaction systems for other metal ions. The absorption spectra and reactivities of the SAT complexes for various M^{2+} ions are useful for elucidating the structural characteristics of the porphyrin core in the SAT complex and the overall metalation mechanism. The metalloporphyrins with an oxidized metal(III) center are formed by reactions between the porphyrins and Mn^{2+} or Co^{2+} under aerobic conditions,[13,14] and then this oxidation behavior must be related to the nature of the SAT complexes formed during their dynamic processes. Therefore, in this study, the characterization of the SAT complex of a series of M^{2+} ions (Mn^{2+}, Fe^{2+}, Co^{2+}, Ni^{2+}, Cu^{2+}, and Zn^{2+}) has been spectrophotometrically carried out in AN and the formation rates of the SAT complexes have been determined in order to clarify the difference among the M^{2+} ions with respect to the rate of the subsequent metalloporphyrin formation. We will propose a unified mechanism of metalloporphyrin formation by comparison with the solvent exchange on M^{2+} ions.

Structural information on the SAT complex is very important for understanding the formation and deprotonation mechanisms of the SAT complex. However, it is difficult to isolate single crystals of the SAT complexes for these M^{2+} ions, and we have not yet succeeded. The extended X-ray absorption fine structure (EXAFS) method is the most powerful technique to determine the local structure around the metal center in solution. We then applied this technique to the structural analysis of the Cu(II)−SAT complex formed in AN because the Cu(II)−SAT complex is the most stable among the above M^{2+} ions and the subsequent deprotonation reaction to form the metalloporphyrin can be interrupted for water concentrations less than 5×10^{-3} mol kg^{-1}. The solubility of H_2tpp is fairly low in AN, and we overcame this disadvantage by measuring the fluorescent EXAFS spectrum of the Cu(II)−SAT complex in AN together with those of some other Cu^{2+} complexes with different geometries around the Cu^{2+} ion in order to compare the X-ray absorption near-edge structure (XANES). This is the first report on the structure around the metal center in the SAT complex as a reaction intermediate formed during the dynamic process of the metalation reaction.

Experimental Section

Materials. Acetonitrile (Wako Pure Chemical Co., Japan) was dried over activated 4 Å molecular sieves for several days and distilled at 110 °C under a nitrogen atmosphere. H_2tpp (Dojin Laboratories, Japan) was used without further purification because the existence of impurities such as 5,10,15,20-tetraphenylchlorine was spectrophotometrically confirmed to be negligible.

To prepare $M(H_2O)_6(CF_3SO_3)_2$, a small excess of CF_3SO_3H (98%, Wako) was added dropwise into manganese(II) carbonate (99.9%, Wako), iron sponge (99.9%, Wako), basic cobalt(II) carbonate (Wako), basic nickel(II) carbonate (Wako), copper(II) oxide (99.99%, Wako), and zinc metal (99.999%, Wako) suspended in water, respectively. Each solution was stirred for 1 day, the residues were filtered, and the resultant solution was then concentrated to obtain pink (Mn^{2+}), pale-blue (Fe^{2+}), red (Co^{2+}), green (Ni^{2+}), blue (Cu^{2+}), and white (Zn^{2+}) crystals of $M(H_2O)_6(CF_3SO_3)_2$. In the case of the ferrous salts, all procedures were performed under an argon atmosphere to prevent the oxidation of the Fe^{2+} ion. The contained water was completely removed by heating each $M(H_2O)_6(CF_3SO_3)_2$ at 250 °C, and the powder of the anhydrous trifluoromethanesulfonate salt, $M(CF_3SO_3)_2$, was obtained. Since the anhydrous salt of Ni^{2+} was not dissolved in AN, $Ni(an)_6(CF_3SO_3)_2$ was prepared by removing the water during reflux of an AN solution of $Ni(H_2O)_6(CF_3SO_3)_2$ for about 5 h in a modified Soxhlet extractor with 4 Å molecular sieves.[15] $Cu(an)_4ClO_4$ prepared by the reduction of $Cu(H_2O)_6(ClO_4)_2$ by copper metal (99.9%, Wako) in AN and $AgNO_3$ (99.9%, Wako) was used as the source of the Cu^+ and Ag^+ ion in AN, respectively. Cu(tpp) were prepared according to previously reported methods.[16] The methanol solution of copper(II) chloride and dmp (dmp = 2,9-dimethyl-1,10-phenanthroline) was concentrated, followed by addition of the dichloromethane solution of $LiBF_4$ to obtain $Cu(dmp)_2(H_2O)(BF_4)_2$.[17]

Preparation of Sample Solutions. Since the equilibrium constant of the Cu(II)−SAT complex formation in AN is greater than 10^7 mol^{-1} kg according to the previous results,[11] the sample solution of the Cu(II)−SAT complex for the fluorescent EXAFS measurements was prepared by dissolving an equivalent amount (1.06×10^{-3} mol kg^{-1}) of $Cu(CF_3SO_3)_2$ and H_2tpp in AN, where the Cu(II)−SAT complex was quantitatively formed. The concentrations of $Cu(an)_6^{2+}$, Cu(tpp), and $Cu(dmp)_2^{2+}$ in the sample solutions for the fluorescent EXAFS measurements were 1.06×10^{-3}, 1.01×10^{-3}, and 1.05×10^{-3} mol kg^{-1}, respectively. The sample solution of Cu(tpp) was prepared in pyridine (Wako), purified by distillation after dehydration using 4 Å molecular sieves due to the low solubility of Cu(tpp) in AN, while the other sample solutions were made using AN as the solvent.

Sample solutions for the spectrophotometric and kinetic measurements were prepared by dissolving the corresponding metal salts in AN under a nitrogen atmosphere in order to prevent contamination by water in the air. The water content in the sample solutions was confirmed to be less than 5×10^{-3} mol kg^{-1} by the Karl−Fisher method.

Fluorescent EXAFS Measurements and Data Analysis. The fluorescent EXAFS spectra in the vicinity of the Cu K edge were measured at the BL-12C station of the Photon Factory of the High Energy Acceleration Research Organization using an ionization chamber filled with N_2 gas and a 19-element solid-state detector as the detectors of the incident and fluorescent X-ray intensities (I_0 and I_f), respectively.[18,19] The monochromatized X-ray using a Si(111) double crystal, which was detuned to 80% of the maximal intensity at the K edge of Cu in order to remove the higher-order reflection, irradiated a sample solution with an incident angle of 45°, and the fluorescent X-ray was monitored in the orthogonal direction of the excitation X-ray. The X-ray

(13) Buchler, J. W. *Porphyrins and Metalloporphyrins*; Smith, K. M., Ed.; Elsevier: Amsterdam, 1975; p 157.
(14) Buchler, J. W. *The Porphyrins*; Dolphin, D., Ed.; Academic Press: New York, 1978; Vol. I, Part A, p 389.
(15) Ishii, M.; Funahashi, S.; Ishihara, K.; Tanaka, M. *Bull. Chem. Soc. Jpn.* **1989**, *62*, 1852.
(16) Fleischer, E. B.; Miller, C. K.; Webb, L. E. *J. Am. Chem. Soc.* **1964**, *86*, 2342.
(17) Hall, J. R.; Marchant, N. K.; Plowman, R. A. *Aust. J. Chem.* **1962**, *15*, 480.
(18) Nomura, M.; Koyama, A. KEK Report 95-15; National Laboratory for High Energy Physics: Tsukuba, Japan, 1995.
(19) Nomura, M. *J. Synchrotron Radiat.* **1999**, *5*, 851.

energy was calibrated by the spectrum of Cu foil. The fluorescent X-ray spectra of solvent were separately measured and subtracted from those of the sample solution by referring to the intensity of the incident X-ray to correct the background intensity of the fluorescent X-ray.

The background-corrected fluorescent EXAFS spectra are shown in Figure S1 (S: Supporting Information). The smooth background in the postedge region was estimated by the cubic spline function using the program REX (Rigaku)[20] to obtain the normalized EXAFS oscillation ($\chi(k)$). The k^3-weighted $\chi(k)$ curves are shown in Figure S2. The obtained $k^3\chi(k)$ values and the k^3-weighted theoretical function of the EXAFS oscillation expressed by

$$\chi(k) = \sum_j \frac{F_j(k) S_{0,j}{}^2 N_j}{kR_j{}^2} \sin(2R_j k + \delta_j(k)) \exp\left(-2k^2\sigma_j{}^2 - \frac{2R_j}{\lambda_j(k)}\right) \quad (2)$$

were converted in R space by Fourier transformation in the range $2.0 < k < 14.5$ Å^{-1} using the Hanning type window function with a width of 0.5 Å^{-1}. $F_j(k)$ is the scattering amplitude from each of the N_j scatterers at distance R_j from the X-ray absorbing atom, $\delta_j(k)$ is the total phase shift, $S_{0,j}{}^2$ is the dumping factor, $\lambda_j(k)$ is the mean free path of a photoelectron, and $\sigma_j{}^2$ is the mean square displacement of R_j. The values of $F_j(k)$, $\delta_j(k)$, and $\lambda_j(k)$ were calculated on the basis of the crystal structures of Cu(tpp),[8] $Cu(an)_4(pz)(BF_4)_2$ (pz = pyrazine),[21] and $Cu(dmp)_2(H_2O)(CF_3SO_3)_2$[22] as the structural standard for the interaction with the pyrrolenine group, AN, and dmp in solution, respectively, using the program FEFF.[23] The nonlinear least-squares calculations were carried out in the range $1.0 < R < 4.0$ Å in order to optimize the values of N_j, R_j, and $\sigma_j{}^2$ by the program FEFFIT.[24]

Spectrophotometric and Kinetic Measurements. UV−vis absorption spectra were recorded on UV−vis spectrophotometers (UV-1600PC, Shimadzu or V-570, Jasco) at 25.0 °C, and spectral changes for the fast reactions in the wavelength range from 400 to 600 nm were measured by a stopped-flow rapid detection system (RSP-600-06, Unisoku). The absorbance changes for the reactions of M^{2+} ions with H_2tpp in AN were followed at 438, 440, 440, and 438 nm for the Mn^{2+}, Co^{2+}, Ni^{2+}, and Zn^{2+} systems, respectively, after mixing the AN solutions of H_2tpp and a large excess of each M^{2+} ion. The temperature of all measurements was maintained at 25.0 ± 0.1 °C by circulating thermostated water.

Results and Discussion

Structure of the Cu(II)−SAT Complex. The X-ray absorption near-edge structure (XANES) spectra of the Cu(II)−SAT complex as well as Cu(tpp), $Cu(dmp)_2{}^{2+}$, and $Cu(an)_6{}^{2+}$ are shown in Figure 1, in which the previously measured spectrum of $Cu(an)_4{}^+$ was included.[25] Although the geometry around the Cu^{2+} ion of $Cu(dmp)_2{}^{2+}$ in AN has not been confirmed, it is suggested that one AN solvent molecule is bound to the Cu^{2+} ion to form $Cu(dmp)_2(an)^{2+}$ with a trigonal bipyramidal geometry, judging from the structures of the crystals containing the $Cu(dmp)^{2+}$ moiety,[22,26−29] and will be discussed on the basis of analysis of the EXAFS in the last paragraph of this section. The XANES spectrum of the Cu(II)−SAT complex is evidently

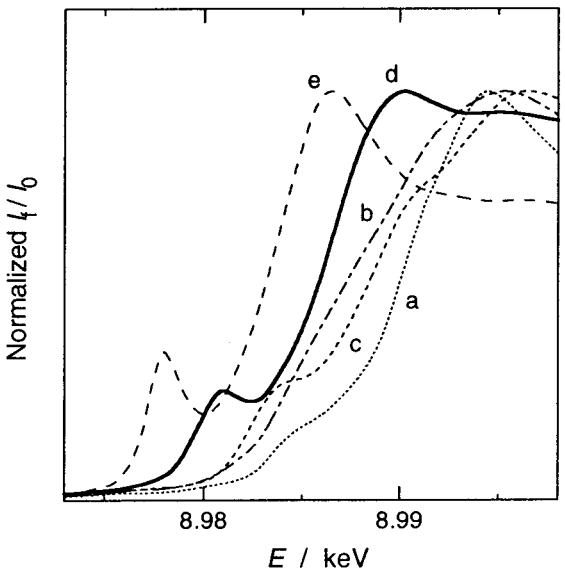

Figure 1. X-ray absorption near-edge structure spectra of $Cu(an)_6{}^{2+}$ in acetonitrile (a), $Cu(dmp)_2(an)^{2+}$ in acetonitrile (b), Cu(tpp) in pyridine (c), the Cu(II)−SAT complex in acetonitrile (d), and $Cu(an)_4{}^+$ in acetonitrile (e).

different from those of the square planar Cu(tpp),[8] axially elongated octahedral $Cu(an)_6{}^{2+}$,[30,31] trigonal bipyramidal $Cu(dmp)_2(an)^{2+}$, and tetrahedral $Cu(an)_4{}^+$.[25,31,32] The difference indicates that the geometry around the Cu^{2+} center of the Cu(II)−SAT complex is different from the axially elongated octahedral, trigonal bipyramidal, and square planar geometries and may be more distorted. The facts that the threshold X-ray energy of the Cu(II)−SAT complex is relatively similar to those of the divalent Cu^{2+} compounds and that there is a clear discrepancy between the divalent compounds and the monovalent compound $Cu(an)_4{}^+$ prove that the copper center in the Cu(II)−SAT complex is not reduced, remaining divalent.

Figure 2 shows the absolute parts of the Fourier transform magnitudes of the Cu(II)−SAT complex, Cu(tpp), and $Cu(an)_6{}^{2+}$. Although the main peaks around 1.6 Å (phase shift uncorrected), which mainly arise from the Cu−N bonding interactions, are approximately identical, there is a clear difference in the longer region (2.0−4.0 Å), where the nonbonding interactions and multiple scatterings are effective. The characteristic peak at 2.5 Å with the shoulder at 2.1 Å is observed in the Fourier transform of $Cu(an)_6{}^{2+}$, while there are more complicated features with the peaks at 2.2, 2.6, 2.9, 3.3, and 3.8 Å in that of Cu(tpp). In the case of the Cu(II)−SAT complex, both characteristics observed for $Cu(an)_6{}^{2+}$ and Cu(tpp) appear in the Fourier transforms, and the intensities for each component are almost half the original one. These findings qualitatively indicate that two pyrrolenine groups are bound to the Cu^{2+} ion in the Cu(II)−SAT complex, and this is consistent with the result of the previously reported ^{1}H NMR.[11]

The N values for all the interactions were fixed for analysis of the EXAFS spectra of $Cu(an)_6{}^{2+}$, $Cu(dmp)_2(an)^{2+}$, and Cu(tpp), and the values of R, σ, $S_0{}^2$, and the threshold energy correction, ΔE_0, were optimized as variables. The obtained values for the bonding interactions around the Cu^{2+} ion are summarized in Table 1 together with some reported values for

(20) Teranishi, T.; Harada, M.; Asakura, K.; Asanuma, H.; Saito, Y.; Toshima, N. *J. Chem. Phys.* **1994**, *98*, 7967.
(21) Begley, M. J.; Hubberstey, P.; Stroud, J. *J. Chem. Soc., Dalton Trans.* **1996**, 2323.
(22) Tran, D.; Skelton, B. W.; White, A. H.; Laverman, L. E.; Ford, P. C. *Inorg. Chem.* **1998**, *37*, 2505.
(23) Zabinsky, S. I.; Rehr, J. J.; Ankudinov, A.; Albers, R. C.; Eller, M. *J. Phys. Rev. B* **1995**, *52*, 2995.
(24) Newville, M.; Ravel, R.; Haskel, D.; Rehr, J. J.; Stern, E. A.; Yacoby, Y. *Phys. B* **1995**, *208/209*, 154.
(25) Inada, Y.; Tsutsui, Y.; Wasada, H.; Funahashi, S. *Z. Naturforsch.* **1999**, *54b*, 193.
(26) Marsh, R. E. *Acta Crystallogr. B* **1997**, *53*, 317.
(27) Heldal, H. E.; Sletten, J. *Acta Chem. Scand.* **1997**, *51*, 122.
(28) Simmons, C. J.; Lundeen, M. Seff, K. *Inorg. Chem.* **1978**, *17*, 1429.
(29) Preston, H. S.; Kennard, C. H. L. *J. Chem. Soc. A* **1969**, 2955.
(30) Funahashi, S.; Inada, Y. *Trends Inorg. Chem.* **1998**, *5*, 15.
(31) Persson, I.; P.-Hahn, J. E.; Hodgson, K. O. *Inorg. Chem.* **1993**, *32*, 2497.
(32) Csöregh, I.; Kierkegaard, P.; Norrestam, R. *Acta Crystallogr. B* **1975**, *31*, 314.

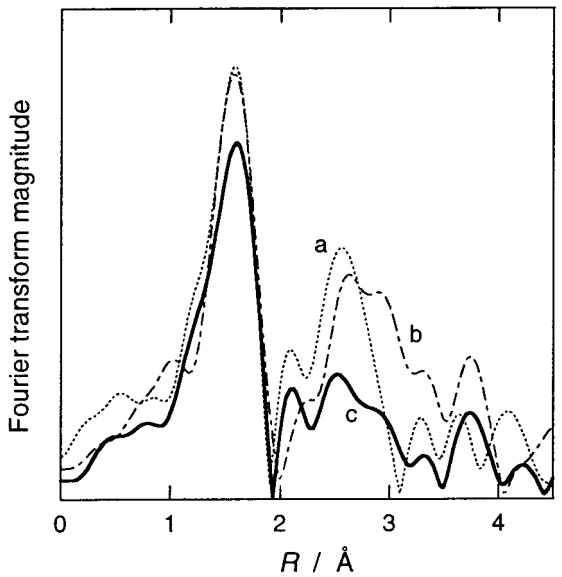

Figure 2. Absolute parts of the Fourier transform magnitudes of $Cu(an)_6^{2+}$ (a), Cu(tpp) (b), and the Cu(II)−SAT complex (c).

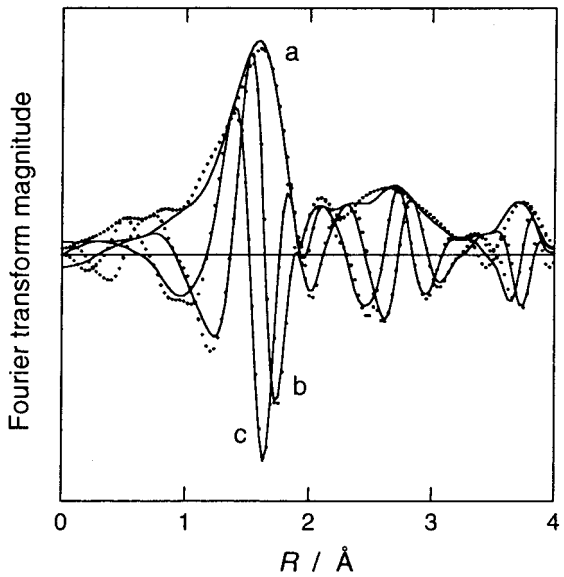

Figure 3. Fourier transform magnitudes of the Cu(II)−SAT complex in acetonitrile. The absolute values (a) of the observed data are shown by dots together with their imaginary (b) and real (c) parts. Calculated results using the obtained parameters are represented by solid lines.

Table 1. Structure Parameters around the Cu^{2+} Ion As Determined by Fluorescent EXAFS[a]

complex	interaction	*N*	*R*/Å
$Cu(H_2tpp)(an)_4^{2+}$	Cu−N(pyr)[b]	1.6	2.05
	$Cu-N(an)_{eq}$[c,d]	2.4	1.98
	$Cu-N(an)_{ax}$[c,e]	2.4	2.32
Cu(tpp)	Cu−N(pyr)[b]	4[f]	2.02
Cu(tpp)[g]	Cu−N(pyr)[b]	4	1.98−2.01
$Cu(an)_6^{2+}$	$Cu-N(an)_{eq}$[c,d]	4[f]	1.99
	$Cu-N(an)_{ax}$[c,e]	2[f]	2.40
$Cu(an)_6^{2+}$[h]	$Cu-N(an)_{eq}$[c,e]	4[f]	1.99
	$Cu-N(an)_{ax}$[c,e]	2[f]	2.23
$Cu(an)_4(pz)(BF_4)_2$[i]	$Cu-N(an)_{eq}$[c,d]	2	2.02
	$Cu-N(an)_{ax}$[c,e]	2	2.39
	$Cu-N(pz)_{eq}$[j]	2	2.02[k]
$Cu(an)_4^{+}$[h]	Cu−N(an)[c]	4[f]	2.00
$Cu(an)_4ClO_4$[l]	Cu−N(an)[c]	4	1.99[k]
$Cu(dmp)_2(an)^{2+}$[m]	Cu−N(dmp)[n]	2[f]	1.97
		2[f]	2.20
	Cu−N(an)[c]	1[f]	2.07
$Cu(dmp)_2(H_2O)(CF_3SO_3)_2$[o]	Cu−N(dmp)[n]	2	1.98
		2	2.12
	Cu−O	1	2.08

[a] Errors of *N* and *R* are estimated to be ca. 0.2 and 0.01 Å, respectively. [b] Interaction between Cu and pyrrolenine nitrogen. [c] Interaction between Cu and nitrogen of bound AN. [d] Equatorial site of the Cu(II) ion. [e] Axial site of the Cu(II) ion. [f] Fixed during the least-squares calculation. [g] In single crystal. References 16 and 33−35. [h] Determined by EXAFS measurement in transmission mode. Reference 30. [i] In single crystal. pz = pyrazine. Reference 21. [j] N(pz) denotes the coordinating nitrogen of pz. Equatorial site of the Cu(II) ion. [k] Averaged value. [l] In single crystal. Reference 32. [m] dmp = 2,9-dimethyl-1,10-phenanthroline. [n] N(dmp) denotes the coordinating nitrogen of dmp. [o] In single crystal. Reference 22.

the corresponding and analogous compounds.[16,21,30,32−35] The more complete parameters for all the interactions analyzed in this study are tabulated in Tables S1−S3. The S_0^2 values determined for Cu(tpp) and $Cu(an)_6^{2+}$ were used as constants for the interactions with H_2tpp and AN during the course of the analysis of the EXAFS spectrum, and the other structure parameters of the Cu(II)−SAT complex around the Cu^{2+} ion were optimized by the least-squares calculation. The obtained values are given in Tables 1 and S4. The Fourier transformations of the observed and calculated $k^3\chi(k)$ curves are shown in Figures 3, S3, and S4 for the Cu(II)−SAT complex, $Cu(an)_6^{2+}$, and Cu(tpp), respectively. The *R* values of $Cu(an)_6^{2+}$ determined in this study by the fluorescent EXAFS measurement are in agreement with those obtained by the EXAFS spectrum measured in the transmission mode,[30] and the *R* value (2.02 Å) of Cu(tpp) is in accordance with those in single crystals within the experimental uncertainty.[16,33−35] For the Cu(II)−SAT complex, the observed EXAFS data are satisfactorily reproduced by three kinds of Cu−N interactions with *N* values of ca. 2, i.e., the Cu−N(pyr), $Cu-N(an)_{eq}$, and $Cu-N(an)_{ax}$ interactions with the *N* and *R* values of 1.6 and 2.05 Å, 2.4 and 1.98 Å, and 2.4 and 2.32 Å, respectively, where N(pyr), $N(an)_{eq}$, and $N(an)_{ax}$ respectively mean the coordinating nitrogen atom of H_2tpp, AN at the equatorial site, and AN at the axial site. Interestingly, the *R* value for Cu−N(pyr) in the Cu(II)−SAT complex ($Cu(H_2tpp)(an)_4^{2+}$) is larger than that (2.02 Å) of Cu(tpp), while the *R* value of 1.98 Å for $Cu-N(an)_{eq}$ is almost identical with that (1.99 Å) of the equatorial site of $Cu(an)_6^{2+}$. The longer bond distance of Cu−N(pyr) rather than that of Cu(tpp), in which the Cu^{2+} ion is just incorporated into the porphyrin core, is ascribed to the limitation due to steric geometry of the porphyrin core. Consequently, the bite angle of N(pyr)−Cu−N(pyr) should be much larger than 90°, considering the bidentate coordination of the opposite two pyrrolenine groups of H_2tpp in the Cu(II)−SAT complex, as indicated by the ^{1}H NMR spectrum.[11]

It is well-known that by steric restriction of bound ligands, the geometry around the Cu^{2+} ion is easily varied with a variety of dihedral angles between the two N−Cu−N planes of the equatorial site from 0 to 90°.[36−38] However, the EXAFS spectrum of the Cu(II)−SAT complex was satisfactorily repro-

(33) Bryn, M. P.; Curtis, C. J.; Hsiou, Y.; Khan, S. I.; Sawin, P. A.; Tendick, S. K.; Terzis, A.; Strouse, C. E. *J. Am. Chem. Soc.* **1993**, *115*, 9480.
(34) Bryn, M. P.; Curtis, C. J.; Goldberg, I.; Hsiou, Y.; Khan, S. I.; Sawin, P. A.; Tendick, S. K.; Strouse, C. E. *J. Am. Chem. Soc.* **1991**, *113*, 6549.
(35) Erler, B. S.; Scholz, W. F.; Lee, Y. J.; Scheidt, W. R.; Reed, C. A. *J. Am. Chem. Soc.* **1987**, *109*, 2644.
(36) Miller, M. T.; Gantzel, P. K.; Karpishin, T. B. *Inorg. Chem.* **1998**, *37*, 2285.
(37) Müller, E.; Bernardinelli, G.; Reedijk, J. *Inorg. Chem.* **1996**, *35*, 1952.

duced by the model with an axial Cu−N(an) interaction, and the result is in agreement with that observed for the structure parameters around the Cu^{2+} ion in the Cu(II)/Hg(II) heterodinuclear porphyrin intermediate.[39] Furthermore, the fact that the *R* value of $Cu-N(an)_{eq}$ is almost the same as that of $Cu(an)_6^{2+}$ strongly indicates that the AN molecules coordinate to the Cu^{2+} ion at the equatorial sites in the distorted octahedral environment because the bond distance in the tetrahedral analogue with a reduced coordination number should be shortened, as indicated by the structural data of solvated metal ions with a reduced solvation number in bulky solvents.[40−42] Thus, we can conclude that the dihedral angle around the Cu^{2+} ion in the Cu(II)−SAT complex may be ca. 0°. Therefore, the Cu(II)−SAT complex seems to have an axially elongated and equatorially distorted six-coordinate geometry.

Here, the structure parameters around the Cu^{2+} ion in $Cu(dmp)_2^{2+}$ in AN were determined by analyzing the EXAFS spectrum. The geometry around the Cu^{2+} ion was reported to be trigonal bipyramidal in some single crystals.[22,26−29] The one nitrogen atom of the dmp ligand coordinates to the Cu^{2+} ion at the equatorial site, the other binds to the axial site of the trigonal bipyramid, and the remaining position at the equatorial site is occupied by a solvent molecule or counteranion. Considering that one AN solvent molecule can coordinate to the Cu^{2+} ion in AN, we analyzed the EXAFS spectrum of $Cu(dmp)_2^{2+}$ in AN using two kinds of model structures: one is composed of two Cu−N(dmp), where N(dmp) denotes the coordinating nitrogen atom of dmp, with $N = 2$, and the other contains the additional Cu−N(an) interaction with $N = 1$.[43] Figure S5 shows the Fourier transformations of the observed and calculated $k^3\chi(k)$ curves for these two models. The model without the Cu−N(an) interaction does not reproduce well the observed data (Figure S5B), while the model including the Cu−N(an) interaction has good reproducibility (part A of Figure S5). We then concluded that the coordination number of the Cu^{2+} ion is 5 in AN. The structure parameters of $Cu(dmp)_2(an)^{2+}$ are included in Tables 1 and S2. The *R* values of the Cu−N(dmp) interactions obtained in AN are in agreement with those in the single crystals.[22]

Characterization of SAT Complexes Formed in Acetonitrile. The formation of the SAT complexes was spectrophotometrically confirmed for Mn^{2+}, Fe^{2+}, Co^{2+}, Ni^{2+}, Cu^{2+}, and Zn^{2+}, but no formation was observed for the monovalent Cu^+ and Ag^+ ions. Because the Cu−N(an) bond distance (2.00 Å) of $Cu(an)_4^+$ in AN is shorter than the Zn−N(an) bond distance (2.13 Å) of isoelectronic $Zn(an)_6^{2+}$ in AN,[25,30] the fact that the SAT complex does not form in the case of Cu^+ but does form for Zn^{2+} is interpreted in terms of the lower charge density of the Cu^+ ion. Similarly, it is reasonable that the Ag^+ ion with a much lower charge density does not form the SAT complex.

In the case of Mn^{2+}, Co^{2+}, and Zn^{2+}, the reaction between H_2tpp and M^{2+} in AN proceeds by two steps under the present experimental conditions. Some examples of the UV−vis absorption spectral change corresponding to the first reaction are shown in Figure S6. The spectral changes for the succeeding second reaction are shown in Figure S7. In the first reaction, some isosbestic points are clearly observed and the changes in absorbance as a function of reaction time are first order with respect to both H_2tpp and M^{2+}. The split Soret bands were observed in the absorption spectra of the reaction products for the first reactions for Mn^{2+}, Co^{2+}, Ni^{2+}, and Zn^{2+}, and they are apparently different from those of the metalloporphyrins M^{II}(tpp) and M^{III}(tpp)$^+$, which have the characteristic Soret bands in nm at 435−440 (Mn^{2+}), 380−410 and ∼480 (Mn^{3+}, which has the split band), 410−415 (Co^{2+}), ∼440 (Co^{3+}), ∼415 (Ni^{2+}), and 420−422 (Zn^{2+}) according to the spectral data compiled in Table S5. Furthermore, the reaction time scales on the order of 100 ms (Mn^{2+}), 10 m (Co^{2+}), 10 h (Ni^{2+}), and 1 s (Zn^{2+}) for the first reactions are still shorter than those of the corresponding metalloporphyrin formation rates. It is thus considered that the first reactions of these M^{2+} ions correspond to the formation of the M(II)−SAT complexes as expressed by

$$M^{2+} + H_2tpp \underset{k_d}{\overset{k_f}{\rightleftharpoons}} M(H_2tpp)^{2+} \qquad (3)$$

where k_f and k_d are the rate constants for the formation and dissociation of the SAT complex, respectively. Figure 4 shows the obtained UV−vis absorption spectra for a series of SAT complexes together with that of the Cu(II)−SAT complex reported previously.[11] Since the second reactions succeeded for

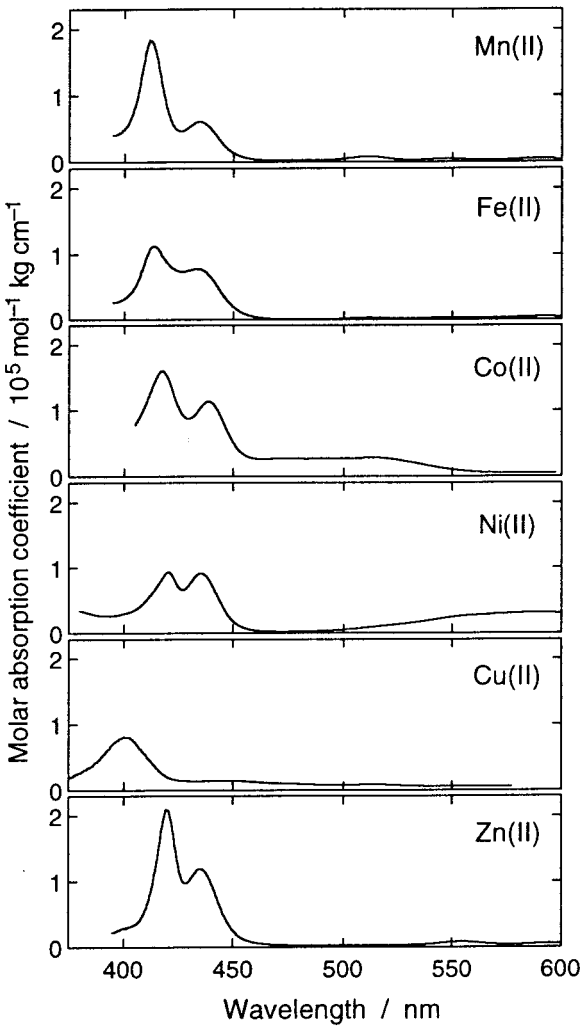

Figure 4. UV−vis absorption spectra of the SAT complexes in acetonitrile.

(38) Adams, H.; Bailey, N. A.; Fenton, D. E.; Moss, S.; Rodriguez de Barbarin, C. O. *J. Chem. Soc., Dalton Trans.* **1986**, 693.
(39) Ohtaki, H.; Inada, Y.; Funahashi, S.; Tabata, M.; Ozutsumi, K.; Nakajima, K. *J. Chem. Soc., Chem. Commun.* **1994**, 1023.
(40) Inada, Y.; Hayashi, H.; Sugimoto, K.; Funahashi, S. *J. Phys. Chem. A* **1999**, *103*, 1401.
(41) Inada, Y.; Sugimoto, K.; Ozutsumi, K.; Funahashi, S. *Inorg. Chem.* **1994**, *33*, 1875.
(42) Ozutsumi, K.; Abe, Y.; Takahashi, R.; Ishiguro, S. *J. Phys. Chem.* **1994**, *98*, 9894.
(43) The analysis using the model with single Cu−N(dmp) interaction with $N = 4$ could not reproduce absolutely the observed data.

Table 2. UV−Vis Spectral Data of SAT Complexes in Acetonitrile

metal(II)	λ_1[a]/nm	λ_2[a]/nm	λ_Q[b]/nm	$\Delta\lambda$[c]/nm
Mn(II)	416	438	512, 544, 587	22
Fe(II)	414	433	511, 547, 593	20
Co(II)	418	439	514, ∼550,[d] 583	21
Ni(II)	424	437	∼518,[d] ∼553,[d] ∼587[d]	13
Cu(II)	402	448	515[e]	46
Zn(II)	420	436	517, 554, 595	16

[a] Absorption peak maximum of the Soret band. [b] Absorption peak maxima of the Q-band observed in the wavelength range shorter than 600 nm. [c] Difference in wavelength between λ_1 and λ_2. $\Delta\lambda = \lambda_2 - \lambda_1$. [d] These peaks overlapped with the d−d transition band of $M(an)_6^{2+}$ (M = Co and Ni). [e] Only one peak was observed.

Mn^{2+}, Co^{2+}, and Zn^{2+}, the spectra shown in Figure 4 are transient, although quantitative formation of the SAT complex was kinetically confirmed. The absorption bands due to the d−d transition of Co^{2+} and Ni^{2+} also appear. The wavelengths of the absorption peak maxima of the SAT complexes are summarized in Table 2.

Although the SAT complex formation rates were confirmed to be independent of small amounts of water less than 10^{-2} mol kg^{-1} in the sample solutions, the behavior of the succeeding second reaction did vary because of the presence of water and oxygen. The succeeding reaction rates of the Zn^{2+} system were accelerated with increasing concentrations of water, and the absorption spectrum of the reaction product for the Co^{2+} system changed in the absence and presence of dissolved oxygen as shown in parts B and C of Figure S7, respectively. It is thus suggested that both the deprotonation to form M(tpp) and the oxidation of the central M^{2+} ion to form $M(tpp)^+$ are included in the succeeding second reaction. The product of the second reaction for the Zn^{2+} system has the absorption peak maximum at 424 nm, and it is in agreement with that of Zn(tpp) (see Table S5). In the case of the Co^{2+} system in the absence of dissolved oxygen, the absorption peak at 439 nm, which is related to the Co(II)−SAT complex, decreases and the peak at 418 nm is shifted to 414 nm. Since Co(tpp) has the characteristic Soret band at 410−415 nm (see Table S5), the reaction product can be assigned to Co(tpp) formed by the deprotonation of the Co(II)−SAT complex under anaerobic conditions. On the other hand, the absorption peak at 434 nm increases and that at 418 nm decreases without deoxygenation. Because the spectral pattern of the reaction product formed under aerobic conditions is very similar to that of CoCl(tpp)(py) in tetrahydrofuran (the Soret band at 439 nm with the shoulder at 416 nm),[44] the product can be assigned to $Co(tpp)^+$. Furthermore, the fact that the reaction time scales to form Co(tpp) and $Co(tpp)^+$ under anaerobic and aerobic conditions, respectively, are comparable indicates that the oxidation occurs on the Co^{2+} center of the Co(tpp) formed by the rate-determining deprotonation of the Co(II)−SAT complex. During the spectral change of the second reaction of the Mn^{2+} system shown in part A of Figure S7, the absorption intensity of the peak at 438 nm, which is related to the Mn(II)−SAT complex, decreases and the peak at 416 nm is shifted to 413 nm with increasing intensity. The Mn(tpp) complex is characterized by the Soret band at 435−440 nm, and the $Mn(tpp)^+$ complex has the split Soret bands at 380−410 and ∼480 nm (see Table S5). The absorption peak observed at 413 nm for the product of the second reaction of the Mn^{2+} system is clearly different from that of Mn(tpp) and $Mn(tpp)^+$. We can thus conclude that the product of the second reaction

Scheme 1

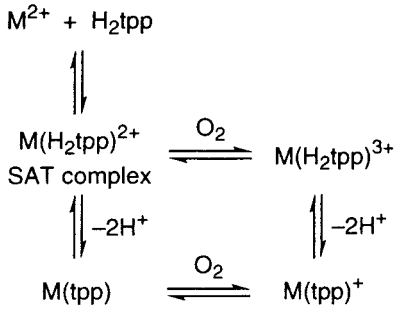

may be the Mn(III)−SAT complex formed by the oxidation of the Mn(II)−SAT complex due to dissolved oxygen. The faster oxidation of the Mn(II)−SAT complex compared with the oxidation of the Co(II)−SAT complex may be due to the lower redox potential of the Mn(II)−SAT complex. The values of redox potential ($E°$) for the $M(H_2O)_6^{3+/2+}$ couple in aqueous solution are reported to be +1.51 and +1.82 V vs NHE for M = Mn and Co, respectively.[45] Assuming that the order in the value is retained for the M(II)−SAT complexes formed in AN, the faster oxidation of the Mn(II)−SAT complex compared with the oxidation of the Co(II)−SAT complex is consistent with the order in the $E°$ values. Therefore, in the present system, $Mn(H_2tpp)^{2+}$ is oxidized, leading to $Mn(H_2tpp)^{3+}$, and Co(tpp) is oxidized to form $Co(tpp)^+$. The formation of the Mn(III)−SAT complex preceding the formation of Mn(tpp) suggests that the deprotonation rate of the Mn(II)−SAT complex is slower than that of the Co(II)−SAT complex.

In summary, the reaction between H_2tpp and M^{2+} in AN can be described by Scheme 1 for Mn^{2+}, Co^{2+}, Ni^{2+}, Cu^{2+}, and Zn^{2+}. The SAT complex ($M(H_2tpp)^{2+}$) is formed by the faster first reaction in AN and is finally oxidized by dissolved oxygen to form $M(tpp)^+$ in the case of Mn^{2+} and Co^{2+}, although the deprotonation and oxidation rates of the SAT complexes of Mn^{2+} and Co^{2+} are competitive. The SAT complexes of Ni^{2+} and Cu^{2+} are quite stable, and the deprotonation and oxidation reactions do not occur under the present experimental conditions without the Brønsted bases.

The absorption spectra of the product for the reaction between H_2tpp and Fe^{2+} are shown in Figure S8 for a variety of Fe^{2+} concentrations. The wavelength of the isosbestic point around the Soret band is changed from 419 nm for 0 to ca. 7×10^{-4} mol kg^{-1} to 427 nm for greater than a 1×10^{-3} mol kg^{-1} Fe^{2+} concentration. This indicates that there are two step reactions with respective participation of distinct Fe^{2+} ion for each step. The absorption peak maximum at 440 nm of the product for the second reaction is clearly different from those of Fe(tpp) and $Fe(tpp)^+$, which have characteristic peaks at ∼425 and 410−420 nm, respectively (see Table S5). The involvement of Fe^{3+} is ruled out because of the high redox potential of the $Fe^{3+/2+}$ couple in AN of 2.00 V (vs NHE in water).[46] In addition, according to our results from preliminary experiments in the presence of *p*-toluenesulfonic acid (Htsa) shown in Figure S9, the absorption spectrum of the second reaction in the absence of Htsa shown in Figure S8 is very similar to that of the reaction product between the porphyrin diacid (H_4tpp^{2+}) and Fe^{2+} but is clearly different from that of H_4tpp^{2+} itself with the peak maximum at 441 nm. Therefore, the product of the second reaction is thought to be $Fe_2(tpp)^{2+}$ and the observed two-step

(44) Kobayashi, H.; Hara, T.; Kaizu, Y. *Bull. Chem. Soc. Jpn.* **1972**, *45*, 2148.
(45) Burgess, J. *Metal Ions in Solution*; John Wiley & Sons: New York, 1978.
(46) Kratochvil, B.; Long, R. *Anal. Chem.* **1970**, *42*, 43.

reactions can be expressed by

$$Fe^{2+} + H_2tpp \underset{k_d}{\overset{k_f}{\rightleftharpoons}} Fe(H_2tpp)^{2+} \quad (4)$$

and

$$Fe^{2+} + Fe(H_2tpp)^{2+} \rightleftarrows Fe_2(tpp)^{2+} + 2H^+ \quad (5)$$

The absorbance data at 416, 425, and 441 nm are plotted as a function of the total concentration of Fe^{2+} (C_{Fe}) in Figure S10. According to these plots, the absorption spectrum observed for $C_{Fe} = (6-7) \times 10^{-4}$ mol kg^{-1} corresponds to that of the Fe(II)−SAT complex formed by eq 4, and thus, the absorption spectrum obtained for $C_{Fe} = 6.31 \times 10^{-4}$ mol kg^{-1} is given in Figure 4 as that of the Fe(II)−SAT complex. The reaction rate of the first reaction corresponding to the Fe(II)−SAT complex formation is too fast to precisely determine the rate constants. The reasons why the dinuclear complex ($Fe_2(tpp)^{2+}$) is formed and the Fe(II)−SAT complex formation is very fast are not given at this stage.

In the UV−vis absorption spectra of the M(II)−SAT complexes for Mn^{2+}, Fe^{2+}, Co^{2+}, Ni^{2+}, Cu^{2+}, and Zn^{2+}, the split Soret bands, of which the peak maxima are referred to as λ_1 and λ_2 ($\lambda_1 < \lambda_2$), are observed as shown in Figure 4 and Table 2. The variations in the λ_1, λ_2, and $\Delta\lambda$ ($=\lambda_2 - \lambda_1$) values for a series of M^{2+} ions are visualized in Figure S11. According to the four-orbital model, the Soret band of H_2tpp is assigned to the $\pi-\pi^*$ electronic transition from the HOMO orbital of $a_{1u}(\pi)$ to the doubly degenerated LUMO orbitals of $e_g(\pi^*)$.[47] This is the case for planar porphyrins and their metalloporphyrins with D_{4h} symmetry. For the latter, the four pyrrole groups are certainly equivalent, and also in the case of the former, the two pyrrole and two pyrrolenine groups become identical because of the fast tautomerism in solution. The single absorption peak of the Soret band is thus observed in these cases because the LUMO orbitals drawn in Figure S12 are energetically identical. The pyrrole and pyrrolenine groups are quite similar in the porphyrin diacid, H_4tpp^{2+}, and a similar single peak of the Soret band is observed for H_4tpp^{2+}, although it is blue-shifted relative to H_2tpp. On the other hand, the split Soret band is observed for some porphyrin derivatives with nonidentical components in the π-electronic system, such as 5,10,15,20-tetraphenylchlorine,[48] 2,3,7,8-tetrahydro-5,10,15,20-tetraphenylporphyrin, and 2,3,7,8,12,13-hexahydro-5,10,15,20-tetraphenylporphyrin.[49] The four five-membered-ring components of the π-electronic system for the porphyrin skeleton are not identical in these cases, and thus, the degeneracy of the LUMO orbitals should be broken. The breakdown of the degeneracy is also evidenced by theoretical calculations.[50,51] In the SAT complexes, two pyrrolenine groups of H_2tpp coordinate to the M^{2+} ion and two protons still remain in the other two pyrrole groups. The symmetry of the porphyrin skeleton should then be lowered from the D_{4h} of H_2tpp to C_{2v} in the SAT complexes. The $e_g(\pi^*)$ orbitals of H_2tpp must be split into the $b_1(\pi^*)$ and $b_2(\pi^*)$ orbitals in the C_{2v} symmetry, and the observed two transitions (λ_1 and λ_2 in Table 2) in the wavelength range 400−450 nm are thus assigned to the transitions from a_{1u} to these orbitals. The energy difference between the $b_1(\pi^*)$ and $b_2(\pi^*)$ orbitals is interpreted to become large with increasing degree of deformation of the porphyrin core. As shown in Table 2 and part A of Figure S11, the $\Delta\lambda$ value slightly decreases with increasing number of d electrons from Mn^{2+} to Zn^{2+} with a great discrepancy for Cu^{2+}. Because the decreasing $\Delta\lambda$ value for a series of M^{2+} ions except for Cu^{2+} is due to both the gradual red shift of λ_1 and the slight blue shift of λ_2 as shown in part B of Figure S11, deformation of the porphyrin core in the SAT complexes becomes smaller from Mn^{2+} to Zn^{2+}. For the Cu(II)−SAT complex, the large blue shift of λ_1 and the red shift of λ_2 are observed relative to the other M^{2+} ions, and thus, the $\Delta\lambda$ value is notably large. This means that the porphyrin core in the Cu(II)−SAT complex is the most deformed. Because the M−N bond distance of 1.99 Å for the equatorial site of $Cu(an)_6^{2+}$ in AN is quite short in comparison with that of 2.22 Å for $Mn(an)_6^{2+}$, 2.14 Å for $Fe(an)_6^{2+}$, 2.11 Å for $Co(an)_6^{2+}$, 2.07 Å for $Ni(an)_6^{2+}$, and 2.13 Å for $Zn(an)_6^{2+}$,[30,52] the large deformation of the porphyrin core in the Cu(II)−SAT complex should be ascribed to the steric requirement to coordinate the shortest equatorial site of the Jahn−Teller distorted Cu^{2+} ion. In addition, according to the extended Hückel calculations for a variety of M(tpp),[53] the energy level of the b_{1g} orbital ($3d_{x^2-y^2}$) for the Jahn−Teller distorted Cu^{2+} ion, which is occupied by one 3d electron, is close to the doubly degenerate LUMO orbitals ($e_g(\pi^*)$) of the porphyrin. The $e_g(\pi^*)$ orbitals are split into the $b_1(\pi^*)$ and $b_2(\pi^*)$ orbitals in the C_{2v} deformed porphyrin, and the $b_1(\pi^*)$ orbital can interact with the b_{1g} orbital of Cu^{2+}. The energy level of the $b_1(\pi^*)$ orbital of porphyrin is raised by the electronic interaction instead of the lowering of the b_{1g} orbital of Cu^{2+}, and the wavelength of λ_1 can also be shortened rather than the other M(II)−SAT complexes. The large deformation of the porphyrin core in the Cu(II)−SAT complex suggested by notably small λ_1 and large λ_2 is then interpreted in terms of both the steric requirement by and electronic interaction with the Jahn−Teller distorted Cu^{2+} ion having a d^9 electronic configuration. For the other metal(II) ions, there is support that the structure of the M(II)−SAT complexes is a six-coordinate distorted octahedron due to steric limitation by coordination of the opposite two pyrrolenine nitrogens as a bidentate ligand.

Kinetics and Mechanisms of the SAT Complex Formation in Acetonitrile. The conditional rate constants, k_{obs}, for the SAT complex formation were determined under the pseudo-first-order conditions with an excess M^{2+} ion concentration, C_M. The plots of k_{obs} against C_M have a linear relation as given in Figure S13. Therefore, under the present experimental conditions, the formation of the SAT complexes is expressed by eq 3 and thus k_{obs} is given by

$$k_{obs} = k_f C_M + k_d \quad (6)$$

For the Mn^{2+} system, because there is a clear intercept in the plot of k_{obs} versus C_{Mn}, the values of k_f and k_d were determined to be 3.4×10^2 mol^{-1} kg s^{-1} and 5.8 s^{-1}, respectively. The formation equilibrium constant ($K = k_f/k_d$) for the Mn(II)−SAT complex was kinetically determined to be 59 mol^{-1} kg at 25 °C. For the other M^{2+} system, since the corresponding plots have a zero intercept, the values of k_f were determined by the slope of the plots in Figure S13, as summarized in Table 3.

In Figure 5 is visualized the trend in variation of the rate constant, k_f, of SAT complex formation in AN for a series of M^{2+} ions and in the rate constant, k_{ex}, of the solvent exchange

(47) Gouterman, M. *The Porphyrins*; Dolphin, D., Ed.; Academic Press: New York, 1978; Vol. III, Part A, p 1.
(48) Dorough, G. D.; Huennekens, F. M. *J. Am. Chem. Soc.* **1952**, *74*, 3974.
(49) Seely, G. R.; Calvin, M. *J. Chem. Phys.* **1955**, *23*, 1068.
(50) Schaffer, A. M.; Gouterman, M. *Theor. Chim. Acta* **1972**, *25*, 62.
(51) Seely, G. R. *J. Chem. Phys.* **1957**, *27*, 125.
(52) Inada, Y.; Sugata, T.; Ozutsumi, K.; Funahashi, S. *Inorg. Chem.* **1998**, *37*, 1886.
(53) Zerner, M.; Gouterman, M. *Theor. Chim. Acta* **1966**, *4*, 44.

Table 3. SAT Complex Formation Rate Constants (k_f) at 25 °C in Acetonitrile Together with the Rate Constants (k_{ex}) for Solvent Exchange on M^{2+} Ions in Some Solvents

	Mn^{2+}	Co^{2+}	Ni^{2+}	Cu^{2+}	Zn^{2+}
k_f/mol^{-1} kg s^{-1}	3.4×10^2	0.18	1.6×10^{-3}	3.6×10^5 [a]	61
k_{ex}/s^{-1}					
in H_2O[b]	3.1×10^7	2.2×10^6	3.8×10^4	4.4×10^9	3×10^7
in MeOH[c]	3.7×10^5	1.8×10^4	1.0×10^3	3.1×10^7	
in DMF[d]	2.7×10^6	3.9×10^5	3.8×10^3	9×10^8	
in AN[e]	1.3×10^7	3.5×10^5	6.2×10^3	$\sim 7 \times 10^8$ [f]	$\sim 5 \times 10^6$ [f]
$\log(k_f/k_{ex})$[g]	−4.6	−6.3	−6.6	−3.3	−4.9

[a] Reference 11. [b] References 54−56 and 58. [c] References 59−61. [d] References 61−64. [e] References 52, 61, and 65−67. [f] Estimated value based on the ratio of k_{ex} in AN to k_{ex} in H_2O for Mn^{2+}, Fe^{2+}, Co^{2+}, and Ni^{2+}. See text. [g] Logarithmic value of k_f devided by k_{ex} in AN.

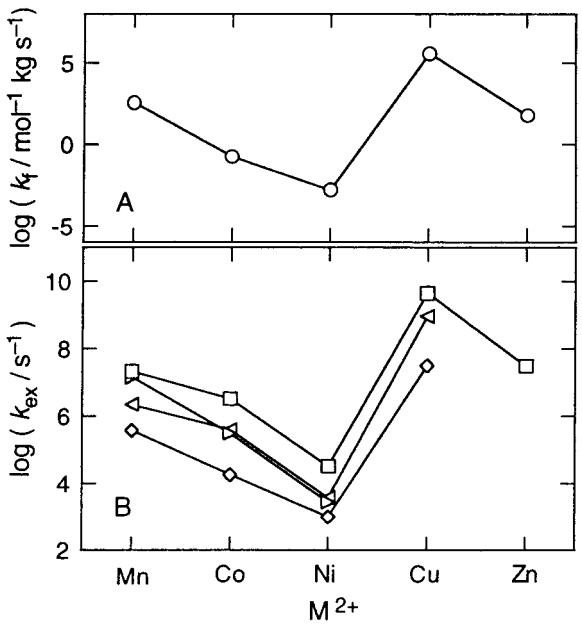

Figure 5. Formation rate constants of the SAT complexes in acetonitrile (A) and solvent exchange rate constants (B). In part B, the values in H_2O, methanol, *N*,*N*-dimethylformamide, and acetonitrile are given by squares, diamonds, left-pointed triangles, and right-pointed triangles, respectively.

in H_2O,[54−58] methanol (MeOH),[59−61] *N*,*N*-dimethylformamide (DMF),[61−64] and AN,[52,61,65−67] of which values are included in Table 3. Unfortunately, although the values of k_{ex} for the solvent exchange on the Cu^{2+} and Zn^{2+} ions in AN are not available, the variation in k_{ex} of a series of M^{2+} ions is similar for various solvents, as expected from Figure 5. Therefore, the observed variation trends in k_f are regarded as being similar to that in k_{ex} for a series of M^{2+} ions. This characteristic strongly indicates that the rate-determining step for the SAT complex formation is similar to that of the solvent exchange; i.e., the rate-determining step of the SAT complex formation is the bond rupture between the M^{2+} ion and a bound AN molecule, simultaneously accompanying the bond formation between the M^{2+} ion and the first pyrrolenine nitrogen of H_2tpp. The chelate ring closure to form the SAT complex, in which H_2tpp is bound to M^{2+} as a bidentate ligand according to the present EXAFS and previous ^{1}H NMR results, must be faster than the rate-determining exchange. The values of k_f are, however, 4−6 orders of magnitude smaller than the k_{ex} values, and thus, it can be expected that there is a large energetic loss due to the fast preequilibria prior to the rate-determining step. If the rapid deformation equilibrium (K_D) of the porphyrin ring and the rapid outer-sphere encounter formation equilibrium (K_{OS}) between the AN-solvated M^{2+} ion and the deformed porphyrin (H_2tpp*) are assumed to precede the rate-determining exchange (reaction 9) between the bound nitrogen of the AN molecule and the first pyrrolenine nitrogen of H_2tpp* as shown by the equations

$$H_2tpp \overset{K_D}{\rightleftharpoons} H_2tpp^* \quad (7)$$

$$M(an)_6^{2+} + H_2tpp^* \overset{K_{OS}}{\rightleftharpoons} M(an)_6^{2+}\cdot H_2tpp^* \quad (8)$$

$$M(an)_6^{2+}\cdot H_2tpp^* \overset{k_{SAT}}{\rightleftharpoons} M(an)_5(H_2tpp)^{2+} + AN \quad (9)$$

and

$$M(an)_5(H_2tpp)^{2+} \overset{fast}{\rightleftharpoons} M(an)_4(H_2tpp)^{2+} + AN \quad (10)$$

then k_f for the formation of the SAT complex ($M(an)_4(H_2tpp)^{2+}$) is expressed by

$$k_f = K_D K_{OS} k_{SAT} \quad (11)$$

The rapid deformation of the porphyrin ring was observed for 5,10,15,20-tetrakis(4-*N*-methylpyridyl)porphyrin in aqueous solution.[68] Because the values of k_f for a series of M^{2+} ions are parallel to the k_{ex} values, the k_{SAT} term in eq 11 may be approximately replaced by k_{ex} in AN. Although the k_{ex} values of Cu^{2+} and Zn^{2+} are not available, it is reasonable that the values of k_{ex} in AN for a series of M^{2+} ions are parallel with those in H_2O, since the AN exchange mechanism of these M^{2+} ions is thought to be the same as that in H_2O. In fact, the values of k_{ex} in AN and H_2O are alike within a factor of 5. The k_{ex} values of Cu^{2+} and Zn^{2+} in AN are respectively estimated to

(54) Ducommun, Y.; Newman, K. E.; Merbach, A. E. *Helv. Chim. Acta* **1979**, *62*, 2511.
(55) Ducommun, Y.; Newman, K. E.; Merbach, A. E. *Inorg. Chem.* **1980**, *19*, 3696.
(56) Hoggard, P. E.; Dodgen, H. W.; Hunt, J. P. *Inorg. Chem.* **1971**, *10*, 959.
(57) Powell, D. H.; Helm, L.; Merbach, A. E. *J. Chem. Phys.* **1991**, *95*, 9258.
(58) Fittipaldi, F.; Petrucci, S. *J. Phys. Chem.* **1967**, *71*, 3414.
(59) Meyer, F. K.; Newman, K. E.; Merbach, A. E. *J. Am. Chem. Soc.* **1979**, *101*, 5588.
(60) Helm, L.; Lincoln, S. F.; Merbach, A. E.; Zbinden, D. *Inorg. Chem.* **1986**, *25*, 2550.
(61) Meyer, F. K.; Newman, K. E.; Merbach, A. E. *Inorg. Chem.* **1979**, *18*, 2142.
(62) Chen, T.-M.; Morgan, L. O. *J. Phys. Chem.* **1972**, *76*, 1973.
(63) Funahashi, S.; Jordan, R. B. *Inorg. Chem.* **1977**, *16*, 1301.
(64) Powell, D. H.; Furrer, P.; Pittet, P.-A.; Merbach, A. E. *J. Phys. Chem.* **1995**, *99*, 16622.
(65) Sisley, M. J.; Yano, Y.; Swaddle, T. W. *Inorg. Chem.* **1982**, *21*, 1141.
(66) Yano, Y.; Fairhurst, M. T.; Swaddle, T. W. *Inorg. Chem.* **1980**, *19*, 3267.
(67) Monnerat, A.; Moore, P.; Newman, K. E.; Merbach, A. E. *Inorg. Chim. Acta* **1981**, *47*, 139.
(68) Pasternack, R. F.; Sutin, N.; Turner, D. H. *J. Am. Chem. Soc.* **1976**, *98*, 1908.

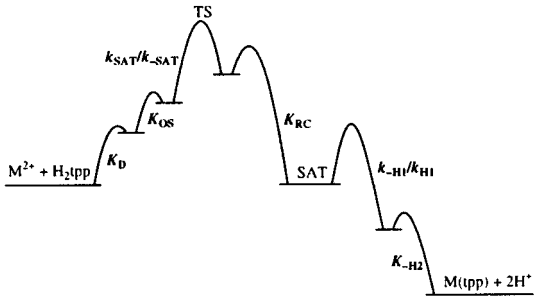

Figure 6. Schematic energy profile of the overall metalation reaction of H_2tpp.

be ca. 7×10^8 and 5×10^6 s^{-1} on the basis of the ratio of the k_{ex} values in AN and H_2O for Mn^{2+}, Fe^{2+}, Co^{2+}, and Ni^{2+}. By division of k_f by k_{ex}, the values of $\log(K_D K_{OS})$ are estimated to be −4.6, −6.3, −6.6, −3.3, and −4.9 for Mn^{2+}, Co^{2+}, Ni^{2+}, Cu^{2+}, and Zn^{2+}, respectively, as given in Table 3. Because the outer-sphere encounter complex is formed by the electrostatic interaction between AN-solvated M^{2+} and H_2tpp*, the magnitude of K_{OS} relates to the charge of both species and their closest approach distance in terms of the Fuoss equation. The variation in the latter for a series of M^{2+} ions is within 10% because the M−N bond distances of AN-solvated M^{2+} ions are not very different.[30,52] The local negative charge, which contributes to the outer-sphere electrostatic interaction, on the pyrrolenine nitrogens of H_2tpp* may vary in response to the degree of deformation of the porphyrin core, but it is improbable that the charge changes by a few factors. The difference in the value of $\log(K_D K_{OS})$ is thus due to the difference in K_D. The notably large K_D value for the Cu^{2+} system reflects the characteristic wavelengths of the split Soret band. The porphyrin skeleton in the Cu(II)−SAT complex is the most deformed among a series of M(II)−SAT complexes. Although the large deformation of the π-electron-conjugated system is unfavorable in enthalpy, it may be effectively compensated in entropy, since significant amounts of freedom in the intramolecular vibration and rotation modes may appear because of the C_{2v} deformation of the porphyrin core.

General Metalation Mechanism. In conclusion, we can generally describe the metalation mechanism on the basis of the present results obtained in AN, as shown in Figure 6. The resolvable elementary reactions during the formation process of the SAT complex are completely expressed by the distortion of the porphyrin ring (K_D), the outer-sphere encounter formation (K_{OS}), the exchange of a bound solvent molecule with the first pyrrolenine nitrogen (k_{SAT}/k_{-SAT}), and the chelate ring closure to form the SAT complex (K_{RC}). In solvents with a higher Brønsted basicity than AN and/or in the presence of bases, which can receive protons, the metalloporphyrin formation proceeds via the first deprotonation of the pyrrole nitrogen in the SAT complex (k_{-H1}/k_{H1}) and the second deprotonation (K_{-H2}). As clarified in this study, the formation rates of the SAT complex are parallel to those of the solvent exchange and the rate-determining step to form the SAT complex is the k_{SAT} step. Therefore, the rate-determining step of the overall metalation reaction is decided by the relative magnitude between k_{SAT} and k_{-H1}. The k_{-H1} value is reasonably interpreted to depend on the Brønsted basicity of the bases. Because the Brønsted basicity of solvents such as H_2O, DMF, and dimethyl sulfoxide, in which the kinetics of many metalation reactions have been examined, is still higher than that of AN, the rate k_{-H1} in such solvents is regarded as being much faster than k_{SAT}. In fact, small amounts of H_2O contained in the sample solution of less than 10^{-2} mol kg^{-1} can receive the pyrrole protons to form the metalloporphyrins in some M^{2+} systems, as observed in this study. The $[H^+]^2$-dependent rate law observed for the demetalation kinetics also supports the fact that the deprotonation steps occur after the rate-determining k_{SAT} step.[69−71] Furthermore, the parallel relation between the metalation rates and the corresponding solvent exchange rates observed for many systems strongly suggests that the k_{SAT} step is rate-determining for the overall metalation process.[72−79]

Acknowledgment. This work was supported by Grants-in-Aid for Scientific Research (Nos. 10440221, 10740305, 10874081, 11354009, and 11554030) from the Ministry of Education, Science, Sports and Culture of Japan and the REIMEI Research Resources of Japan Atomic Energy Research Institute. The EXAFS measurements were performed under the approval of the Photon Factory Program Advisory Committee (Proposal No. 97G054).

Supporting Information Available: Complete lists of the structure parameters around the Cu^{2+} ions in $Cu(an)_6^{2+}$, $Cu(dmp)_2(an)^{2+}$, Cu(tpp), and the Cu(II)−SAT complex (Tables S1−S4), UV−vis absorption spectral data of the metalloporphyrins (Table S5), observed fluorescent EXAFS spectra (Figure S1), observed $k^3\chi(k)$ curves (Figure S2), Fourier transform functions of $Cu(an)_6^{2+}$, Cu(tpp), and $Cu(dmp)_2(an)^{2+}$ (Figures S3−S5), absorption spectral change for the SAT complex formation and its succeeding reaction (Figures S6 and S7), absorption spectra of the reaction product for the Fe^{2+} system (Figure S8), absorption spectral change for the reaction between Fe^{2+} and H_4tpp^{2+} (Figure S9), plots of apparent molar absorption coefficients as a function of total concentration of Fe^{2+} (Figure S10), wavelengths of two peak maxima for the split Soret band and the difference in the wavelength (Figure S11), schematic diagram of the LUMO orbitals of the π-system of porphyrins (Figure S12), and plots of pseudo-first-order rate constants versus the excess M^{2+} ion concentration (Figure S13). This material is available free of charge via the Internet at http://pubs.acs.org.

IC000479W

(69) Shears, B.; Shah, B.; Hambright, P. *J. Am. Chem. Soc.* **1971**, *93*, 776.
(70) Rahimi, R.; Sutter, T. P. G.; Hambright, P. *J. Coord. Chem.* **1995**, *34*, 283.
(71) Tabata, M.; Oshita, K.; Tanaka, M. *Mikrochim. Acta, Wein I* **1985**, 397.
(72) Funahashi, S.; Yamaguchi, Y.; Tanaka, M. *Inorg. Chem.* **1984**, *23*, 2249.
(73) Bain-Ackerman, M. J.; Lavallee, D. K. *Inorg. Chem.* **1979**, *18*, 3358.
(74) Hambright, P.; Chock, P. B. *J. Am. Chem. Soc.* **1974**, *96*, 3123.
(75) Turay, J.; Hambright, P. *Inorg. Chem.* **1980**, *19*, 562.
(76) Choi, E. I.; Fleischer, E. B. *Inorg. Chem.* **1963**, *2*, 94.
(77) Fleischer, E. B.; Choi, E. I.; Hambright, P.; Stone, A. *Inorg. Chem.* **1964**, *3*, 1284.
(78) Kingham, D. J.; Brisbin, D. A. *Inorg. Chem.* **1970**, *9*, 2034.
(79) Tabata, M.; Tanaka, M. *Inorg. Chem.* **1988**, *27*, 203.